J. Phys. B: At. Mol. Phys. **19** (1986) 2547-2564. Printed in Great Britain

Low-energy total cross section measurements for electron scattering from helium and argon

Stephen J Buckman and Birgit Lohmann

Atomic and Molecular Physics Laboratories, Research School of Physical Sciences, Australian National University, Canberra, ACT, Australia

Received 22 October 1985

Abstract. A time-of-flight electron spectrometer has been used to measure absolute total collision cross sections for electrons scattered from helium and argon over the energy range 0.1-20 eV. The measured cross sections are in good agreement with other recent beam experiments and theoretical calculations. At energies below 1 eV modified effective-range theory has been used to enable a comparison of the present work with swarm-derived momentum transfer cross sections. Some limitations of the applicability of the MERT analysis are discussed.

1. Introduction

The measurement of total cross sections for low-energy electron scattering from atoms and molecules has been an important field of experimental endeavour since the earliest experiments of Ramsauer and Kollath (1929), Brüche (1927) and Brode (1925).

The rare gases, particularly helium, have been the subject of extensive study in recent years (see, for example, Jones and Bonham 1982, Nickel *et al* 1985, Ferch *et al* 1985 and references therein). Although accurate total cross section measurements in helium are now available, they are mainly confined to energies above 1 eV, the most recent measurements below 1 eV in helium being those of Ferch *et al* (1980) and Jones and Bonham (1983). An alternative source of information on very-low-energy electron scattering is provided by the analysis of swarm measurements (Crompton *et al* 1970). The cross section derived from such measurements, the momentum transfer cross section, has been obtained in helium at energies as low as 8 meV. A comparison between the momentum transfer cross section derived from swarm data and from total cross section measurements may be made by the use of modified effective-range theory (MERT) (O'Malley 1963).

We present here total cross section measurements for low-energy electron scattering from helium and argon using a new time-of-flight spectrometer. The measurements in helium extend over the energy range 0.1-20 eV, thus providing further experimental data in the region below the maximum in the helium total cross section. In addition the higher-energy data, when compared with the now well established helium cross section, serve as a test of the operation of the new apparatus. The cross section measurements in argon cover the energy range 0.12-20 eV and so include the region of the Ramsauer-Townsend minimum. This energy range has been the subject of much recent experimental (Golden and Bandel 1966, Gus'kov *et al* 1978, Haddad and O'Malley 1982, Jost *et al* 1983, Ferch *et al* 1985) and theoretical (McEachran

0022-3700/86/162547+18$02.50

and Stauffer 1983, Bell *et al* 1984) attention, but it is notable that significant discrepancies still exist in both the magnitude and the position of the Ramsauer-Townsend minimum.

A detailed description of the experimental apparatus is given in § 2. The experimental procedure and the investigation of possible systematic errors are discussed in §§ 3 and 4. The results for helium and argon are presented in § 5, together with a comparison with other recent measurements and calculations of these total cross sections. A comparison is also made with cross sections obtained from swarm data by the application of MERT.

2. Experimental apparatus

The time-of-flight (TOF) spectrometer used in these measurements is similar in many respects to the linear-absorption TOF apparatus of Land and Raith (1974) (see also Ferch *et al* 1980). The scattering apparatus is enclosed in a non-magnetic stainless-steel (grade 310) vacuum envelope which is evacuated using a $330\,l\,s^{-1}$ turbomolecular pump. Base pressures of 1.0×10^{-9} mbar are readily attained. The outer envelope is bakeable to 250 °C.

A schematic diagram of the TOF spectrometer is shown in figure 1. It comprises, basically, an electron source in the form of a tungsten hairpin filament, a number of electron optical elements which will be described in detail later, a beam-pulsing system, a field-free flight tube 255 mm in length and an electron detector, in this case a channel electron multiplier (Mullard B310 BL). The flight tube is machined from a solid block of molybdenum and the inner bore is honed and polished to minimise the effects of surface non-uniformities. The numerous elements which make up the electrostatic

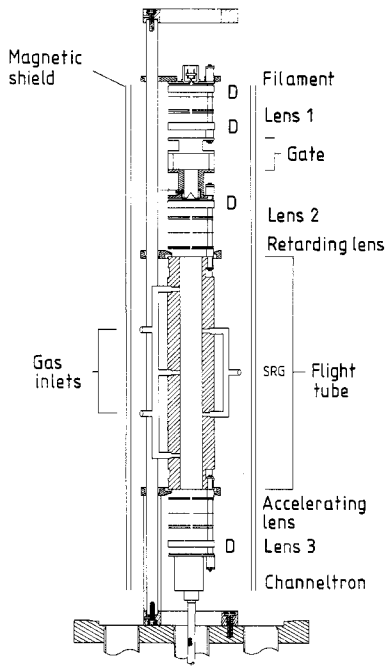

Figure 1. Schematic diagram of the time-of-flight spectrometer. SRG, spinning-rotor viscosity gauge; D, deflector.

aperture lenses are constructed from molybdenum sheet. The beam-gating section is machined from grade 310 stainless steel and those sections which are exposed to the electron beam are lined with molybdenum foil. The rationale behind the extensive use of molybdenum is that it is non-magnetic, high-temperature and high-vacuum compatible and its application in high-resolution electron spectroscopy is well accepted (see, for example, Brunt *et al* 1977). These properties are of particular importance in the present apparatus since the transport of very-low-energy electrons over large distances is dependent on stable, clean surface conditions and low levels of impurities, particularly water vapour. To ensure maintenance of these criteria the electron optics and flight tube are bakeable to 300 °C.

The electron optical system is composed of a number of aperture lenses and deflector systems, all of which are electrostatic. Electrons liberated at the tungsten filament are extracted at an energy of typically 50 eV by a simple triode lens system based on empirical design criteria. The 0.5 mm diameter exit aperture of this lens forms the object of lens 1, a three-element aperture lens ($D = 4$ mm, $A/D = 0.5$ where D is the lens aperture diameter and A the lens element separation), and is imaged onto an aperture of similar size at the entrance of the gating system (see figure 1). This lens also serves to accelerate the electrons to the beam-gating energy which is variable between 50 and 300 eV but is typically 150 eV. The pulsed electron beam which emerges from the gate (to be described in detail later in this section) is then decelerated from the gating energy to a typical energy of 60 eV by lens 2, another three-element aperture lens ($D = 3$ mm, $A/D = 0.5$), and imaged onto the entrance of a compact ($D = 1$ mm, $A/D = 0.5$) four-element 'lens' which serves to provide the major retardation step to the final beam energy in the flight tube (0.1–20 eV). The low-energy electrons enter the flight tube (internal diameter of 26 mm) through a 2 mm diameter aperture and those that emerge from a similar exit aperture are re-accelerated by an identical four-element aperture lens to 60 eV, from where they are accelerated further (typically to 200 eV) by another three-element aperture lens, lens 3 ($D = 3$ mm, $A/D = 0.5$). This lens also focuses the beam into the channeltron detector. The design of the three-element aperture lenses was based on the parameters of Harting and Read (1976). Particular attention was paid to the position of the defining apertures in lens 1 and the gating system to minimise the beam angle. The minimisation of the beam angle at this stage is important for the effective operation of the four-element retarding system where the large deceleration ratios required for low-energy operation are accompanied by a concomitant increase in beam angle and thus a loss of signal. In addition to the electron lenses the electron optical system incorporates four sets of orthogonal deflectors to allow for minor adjustments in the electron beam at various stages of the spectrometer.

The path of the unscattered low-energy electrons within the flight tube is determined entirely by the external electron optics. No magnetic focusing or deflection is employed to modify the electron trajectories within the scattering volume, in contrast to the system employed by Ferch *et al* (1980, 1985). To reduce the effect of the Earth's magnetic field the entire vacuum envelope is contained within a system of three pairs of mutually orthogonal, 2 m diameter Helmholtz coils. This system reduces the ambient terrestrial field at the position of the flight tube to less than 5×10^{-7} T. In addition, within the vacuum envelope but external to the electron optics and flight tube, two concentric cylindrical conetic shields are used to further reduce this field. The Helmholtz coils were adjusted to their final settings by detailed mapping of the magnetic field within the shields with a flux gate magnetometer probe. With these provisions

there was no component of the magnetic field orthogonal to the electron beam greater than 10^{-8} T. As a further safeguard against the effects of local magnetic fields each component of the electron optics was tested with the magnetometer prior to assembly and any stainless-steel parts producing local fields in excess of 2×10^{-9} T were replaced.

The electron beam is shielded from external electrostatic fields by overlapping shielding cylinders which are spot welded to the molybdenum aperture plates. The regions at either end of the flight tube, between the flight tube and the retarding or accelerating lenses, are particularly critical in this respect. Here we have to satisfy the competing criteria of effective electrostatic shielding of the very-low-energy electrons in these regions and the need to maximise the conductance of these regions, in order to efficiently remove the target gas flowing from the flight tube apertures. This is achieved by the use of fine molybdenum mesh cages between the flight tube apertures and the adjacent lens apertures.

An essential aspect of the time-of-flight method is the gating of the electron beam to provide a timing mark for the start of the flight time measurement. (See the review article of Raith (1976) for a comprehensive survey of all aspects of time-of-flight spectroscopy.) In the present system the electron beam is pulsed in a similar fashion to that employed by Kennerly (1978). An RF square-wave pulse applied to a pair of deflection plates sweeps the electron beam across a small (0.3 mm diameter) aperture in the apex of a molybdenum cone. After a time equal to approximately half the width of the original pulse (approximately 1 μs), a second pulse is applied to a second, orthogonal pair of plates, the net effect of the leading and trailing edges of both pulses being to sweep the beam in a rectangular path with one side passing over the gate aperture. The nature of the electron pulse formed by this RF gating procedure depends on the rise time and amplitude of the main pulse as well as the gate energy and physical dimensions of the gating system and electron beam. In our present system, the ability to vary the gate energy from 50 to 300 eV, and the rise time and amplitude of the main pulse from 3 to 15 ns and 2 to 18 V respectively, results in a possible range of electron pulse widths of 0.5–10 ns.

The leads carrying the RF power to the plates enter the vacuum chamber through long re-entrant feedthroughs which allow correct impedance termination of the pulse leads at the gate.

The total cross section is determined by measurements of the transmitted electron intensity with and without gas in the flight tube (see § 3). In the present apparatus gas is admitted to the flight tube via three 6 mm diameter inlet holes. The junctions in the external gas manifold are configured in such a way that the flow through each of these three holes is equal. The gas pressure in the tube is sampled at two points which are vertically and radially offset from the three gas inlet holes. The pressure is measured by a spinning-rotor viscosity gauge (Leybold-Heraeus Viscovac VM211) attached to a common line from the two sampling ports. The pressure in the main vacuum vessel is measured by a nude ionisation gauge. To maintain stability of the filament during measurements both with and without gas flow to the flight tube, the pressure in the region of the filament and electron optics must remain constant. In our case this is achieved by re-directing the gas flow from the flight tube to two small nozzles positioned at the ends of the flight tube, which are designed to simulate the gas leakage from the flight tube through the end apertures when the tube is filled with gas. Switching of the gas flow from one mode to the other is achieved by pneumatically operated high-vacuum valves. We also have the ability to control the gas flow to the flight tube or to the nozzles by the use of a servo-valve (Granville-Phillips APC 216)

and thus ensure that the pressure in the main vacuum vessel remains constant when changing between the two modes of operation. In practice we find that the nozzles mimic the gas flow from the flight tube end apertures so well that no servo-control of the gas flow is needed.

It is important that the gas effusing from the flight tube apertures be pumped efficiently so that scattering in these regions is negligible compared with that in the flight tube. As mentioned previously, molybdenum mesh cages with high transparency are used to provide the necessary electrostatic screening around the entrance and exit apertures with minimum impedance to the gas flow. In the present design the retarding and accelerating lenses are spaced 9 mm from the ends of the flight tube. This arrangement, which is similar to that of the modified flight tube of Ferch *et al* (1985), was arrived at following similar but quite independent considerations of field penetration at the region of non-zero gas density, the effects of which these authors have recently discussed in some detail. Typical operating pressures in the flight tube are in the range $(3.0\text{–}30.0)\times10^{-4}$ mbar and the pressure ratio between the flight tube and vacuum chamber is greater than 150 for both helium and argon.

The temperature of the flight tube is measured at three positions along its length by platinum resistance thermometers (PRT) affixed to the surface of the tube. The outputs of the PRT are monitored using a Leeds and Northrup precision AC bridge. The flight tube temperature is generally 20–22 °C above that of the laboratory (23 °C) due to radiation from the filament and the re-entrant RF pulse lead terminators. To minimise the effects of thermal transpiration the spinning-rotor gauge (SRG) is thermally stabilised at 43 °C. A correction for any resulting temperature differential (greater than 2 °C) between the flight tube and SRG is then made using the empirical expression developed by Takaishi and Sensui (1963) which has recently been confirmed experimentally by Poulter *et al* (1983) for a range of gases.

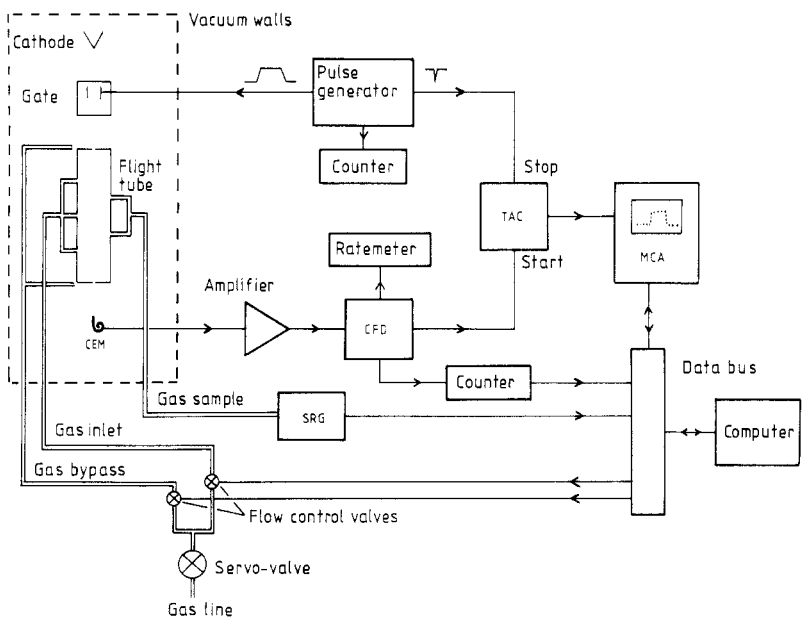

Figure 2. Schematic diagram of the experimental layout.

Conventional fast-timing electronics are used in this experiment to process the timing information from the spectrometer. A schematic diagram of the experimental layout is shown in figure 2. Pulses from the channeltron detector are pre-amplified and processed by a constant-fraction discriminator (CFD) before being used as the start input for a time-to-amplitude converter (TAC). A fast trigger pulse produced simultaneously with the RF beam-gating pulse is used as the stop input for the TAC. This so-called 'inverted-timing' mode will be discussed further in the next section. The output of the TAC is processed by a multichannel analyser (MCA) operating in the pulse height analysis mode.

As the count rates for this type of experiment are often very low, particularly at low energies, long data collection times are required to obtain good statistical accuracy. To alleviate the associated tedium of such experiments and to assist in the reduction of systematic errors the entire experiment, including the operation of the MCA, the pneumatic valves, pressure measurement in the flight tube and data processing, is under computer control.

3. Experimental procedure

The attenuation of a beam of electrons by a target gas is given by the Beer–Lambert relation

$$I = I_0 \exp(-\sigma_T nl) \tag{1}$$

where I_0 is the initial unscattered intensity of the electron beam, I is the intensity of the beam after traversing the scattering medium, n is the number density of the target gas, l is the length of gas through which the electrons travel and σ_T is the total cross section. The total cross section is determined by measurements of the transmitted electron beam intensity with and without the presence of the target gas. Strictly speaking the product nl in the above equation should be replaced by the quantity

$$nl_{\text{eff}} = \int_g^D n(z)\,\mathrm{d}z \tag{2}$$

where l_{eff} is the effective scattering cell length and $n(z)$ is the axial gas density distribution, and the limits of integration are from the beam gate to the detector. This integral is intended to account for pressure gradients within the scattering cell as well as any possible end effects at the entrance and exit apertures. Its evaluation has been approached in several different ways by various experimental groups depending on the assumptions and approximations that can be made for any particular experimental arrangement.

For the present arrangement we can restrict the limits of integration in equation (2) to the region between the retarding and accelerating lenses at either end of the flight tube (see figure 1) since the pressures external to these regions are constant for both gas and reference measurements. Calculations based on the work of Howard (1961) and Mathur *et al* (1975) indicate that end effects will be negligible if, as in the present experimental geometry, the flight tube field-free region extends past the end apertures. In this case the effects of the decrease of the gas number density near the apertures inside the cell are balanced by the non-zero pressure outside the cell, adjacent to the apertures. Our calculations indicate that the correction factor α, where $l_{\text{eff}} = \alpha l$, is unity. This calculation assumes, of course, that there are no other axial pressure

gradients within the scattering cell and that the measured pressure is a true indication of the real cell pressure. These requirements are met in the present apparatus by the use of the three gas inlet pipes and two offset sampling holes described in § 2 and by ensuring that the conductivities of the pipes feeding the three inlet holes from a common supply line are equal.

In a time-of-flight spectrometer, the absolute energy of the electrons as they pass through the target gas is determined from the time they take to traverse the path length l. In this experiment the *measured* time is that between the production of a pulse of electrons at the exit of the gating region and the detection of an electron at the channeltron. Determination of the electron flight times within the field-free region of the drift tube therefore requires an accurate knowledge of the electron flight times through the three-element and four-element lenses, as these times must be subtracted from the measured time. The electron flight times through the three-element lenses are calculated using the axial potential functions of Read (1969, 1970) to determine the axial potential distribution. For the four-element retarding and accelerating lenses we use Bertram's method (1942) to calculate the axial potential, and hence the flight times. The total calculated flight time outside the flight tube is of the order of 30 ns. For electrons of 1.5 eV energy (the highest energy at which we use the TOF method to determine the energy) the flight time through the flight tube is about 370 ns.

In order to assess the accuracy of the axial potential distributions, and hence of the calculated flight times outside the drift tube, these distributions were used in conjunction with the simple ray-tracing method of Kisker (1982) to calculate the lens parameters (focal and mid-focal lengths) for the various three-element lenses. The agreement between these calculations and the tabulated values of Harting and Read (1976) was, in all the cases considered, within 2%. As these calculations were not applied to all possible lens-operating conditions we assume a worst-case error of 10% in the calculated flight times external to the flight tube. This implies, at most, a 1% error in the total calculated flight time at an energy of 1.5 eV, and this percentage error of course decreases as the electron energy with the flight tube is lowered.

The shape and width of the timing spectra depend on a number of experimental parameters, including the gating energy, the mean flight tube energy, the slew rate of the gate pulse, the energy spread in the beam as a result of thermal- and electron-optical-induced effects, and the instrumental timing resolution. The timing resolution, which is comprised principally of jitter in the timing electronics and transit time spread in the channeltron, can be determined by accumulating a timing spectrum at a high energy (200 eV) where the contribution to the width from all other effects can be minimised. Under such optimum conditions we have obtained a timing resolution of 410 ps (figure 3(a)). This value, which is particularly low for a system employing a channeltron, is attributed in part to the use of a coneless variety of channeltron which reduces the contribution to the transit time spread from electrons which strike the periphery of the cone.

The energy resolution of the spectrometer is determined by the timing resolution Δt, the path length uncertainty ΔL and, in the case of helium, a contribution due to Doppler broadening. These contributions are then added in quadrature to obtain the energy resolution. The path length uncertainty is due mainly to field penetration from the accelerating and retarding lenses. We place a conservative estimate on ΔL of 1% of the length L. As a result of these considerations the estimated energy resolution varies from about 3 meV at an energy of 100 meV to 31 meV at 1.5 eV for electron scattering from helium at room temperature.

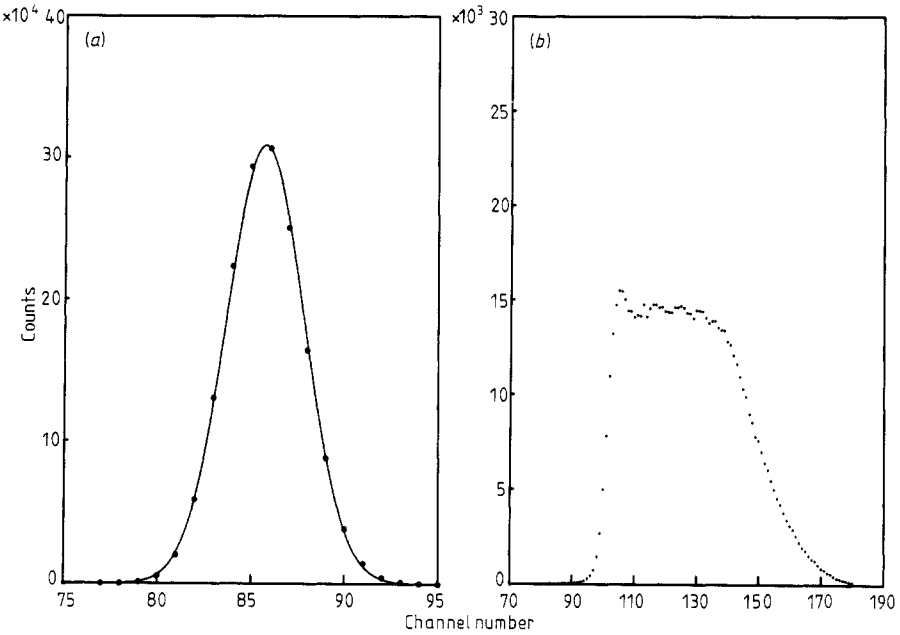

Figure 3. (*a*) Timing spectrum obtained with an electron energy of 200 eV. The full curve is a Gaussian fit to the experimental points with a FWHM of 410 ps. (*b*) Timing spectrum obtained with an average electron energy of 0.4 eV. The spectrum is broadened by the energy width of the emitted electrons from the tungsten filament. The flat, usable portion of the spectrum extends from 0.25–0.60 eV.

The uncertainty in the absolute energy scale arises from uncertainties in the timing calibration procedure (where we essentially measure the fixed delay due to external electronics and calibrate the TAC scale), the error in the lens calculation used to determine the flight time external to the drift tube, and the uncertainty in the length of the field-free region over which the flight time is determined (1%). The resultant total absolute uncertainty is 1.3 meV at an energy of 100 meV and 54 meV at 1.5 eV. At energies above 1.5 eV the absolute uncertainty increases rapidly until at 20 eV it has a value of 3.6 eV. As a result, for all measurements above 1.5 eV, only the peak channel of the narrow Gaussian timing spectra is used as the energy mark and the energy is determined by calibrating the drift tube potential at the mean position of a Gaussian spectrum at an energy of 1 eV, where the absolute uncertainty is 45 meV.

At energies below about 5 eV the thermal spread in the energies (approximately 0.6 eV) of electrons from the hot filament begins to influence the temporal width of the timing spectra. At very low energies (less than 500 meV) judicious adjustment of the electron optics can produce a broad flat spectrum of the type shown in figure 3(*b*).

In order to minimise the possible effects of any long-term drifts in the apparatus each total cross section measurement is carried out by measuring a large number of timing (energy) spectra over the energy range of interest both with and without gas in the flight tube. A typical experimental run consists of, for example, 75 scans with each scan consisting of a 5 min 'gas-in' cycle followed by a (generally) shorter 'gas-out' cycle, so that the statistical accuracy is optimised for a given total counting time. In practice both the total electron count rate and the shape of the energy spectra are extremely stable over periods of up to 18 h. The pressure in the flight tube during the

'gas-in' scan is sampled at 5 s intervals by the spinning-rotor gauge. At each energy at least five, and generally as many as ten, individual cross section measurements have been made over a wide range of electron optical, counting time and gas pressure conditions. The final cross section is determined by taking a weighted mean of all the available data at each particular energy.

Dead-time effects in the MCA are compensated for by using the MCA live time (real time minus dead time) to determine the counting time. The electron count rate (generally 0.1–10 kHz) is such that less than one electron is detected for every 20 electron pulses that emerge from the gate. This ensures that the probability of detecting more than one electron per gate pulse is small.

For background ('gas-out') count rates in excess of 2 kHz, care was taken to ensure that the gas pressure for the signal ('gas-in') measurement was such that the count rates for each measurement were not widely disparate. This was done to minimise any non-linearities in the electron detection channel and TAC. To prevent pulse pile-up problems and to aid in the timing calibration procedure the time-to-amplitude converter is operated in the 'inverted-timing' mode, where the electron pulses are used to start the TAC and the trigger pulses (produced when the electron beam is swept across the gating aperture) are used to stop the TAC.

4. Error analysis

Considerable effort has been made to identify and quantify all the systematic errors in the present work.

Multiple scattering may occur if the gas pressure in the flight tube is too high, allowing the electrons to undergo more than one collision. Under these circumstances the electron may be scattered back out of the flight tube, and subsequently detected as if it were an unscattered electron, thereby resulting in a lowered cross section. In figure 4 the scattering power ($\ln I_0/I$) at several energies is plotted against the measured flight tube pressure for both He and Ar. The pressure dependence is linear over the entire pressure range considered, indicating that the effect of multiple scattering is negligible. Actual operating pressures were always within this range.

Forward-scattered electrons escaping through the exit aperture of the flight tube can also result in a measured cross section which is too small. The solid angle subtended at the detector by the flight tube apertures (at the exit of the flight tube) is very small (2.76×10^{-4} sr). By using elastic and inelastic differential cross sections reported in the literature for both helium and argon (Register *et al* 1980, Nesbet 1979, Chutjian and Cartwright 1981, McEachran and Stauffer 1983, Weyhreter 1983) at a number of energies including the Ramsauer minimum area in argon, we can calculate the reduction in the measured cross section due to forward scattering. These calculations indicate that even by overestimating the differential cross sections by a factor of 10 the error introduced in the total cross section from forward scattering is less than 0.1% over the entire energy range considered here.

As discussed in § 3, the accelerating and retarding regions have been separated from the ends of the flight tube, thereby minimising field penetration into the regions near the exit apertures where the gas pressure is non-negligible. The failure to separate these regions of rapid energy change from those of high gas number density near the flight tube end apertures can result in significant errors in the measured cross section. The magnitude of these errors will depend on the relative values of the lens and flight

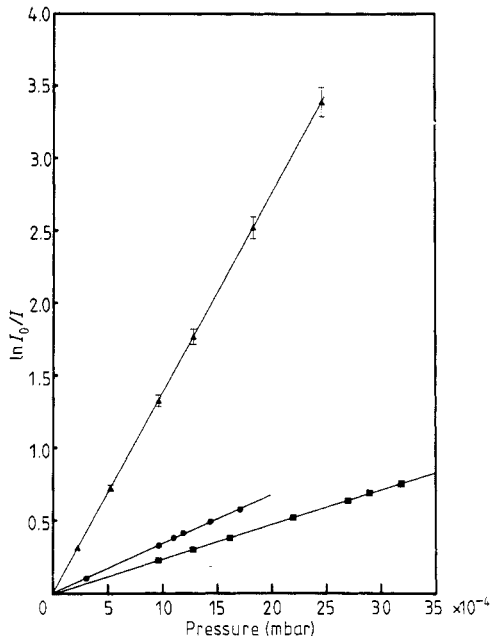

Figure 4. Pressure dependence of the logarithm of the absorption ratio (ln I_0/I) for argon at 14 eV (▲) and helium at 0.15 eV (●) and 12 eV (■). The full curves are linear least-squares fits to the experimental data.

tube voltages and on the target gas. Our studies indicate that the separation of 9 mm between the retarding and accelerating regions and the ends of the flight tube is ample. This assertion is supported by the detailed spectrometer studies of Ferch *et al* (1985). We also investigated the effect on the measured cross section of changes to the potentials on the elements of the retarding and accelerating lenses, and found that a wide variation of potentials had no effect on the value of the measured cross section except at very low energies where it was found that small changes could be induced by excessive (greater than 100 V) voltages on these elements.

As mentioned in § 2, the effect on the measured pressure of the small (less than 2° C) temperature difference between the flight tube and SRG is accounted for by applying the thermal transpiration correction of Takaishi and Sensui (1963). The resultant correction is less than 0.4%. It is difficult to estimate the uncertainty in this correction as thermal transpiration effects are apparatus specific (Baldwin and Gaerttner 1973). The recent measurements by Poulter *et al* (1983) of the thermal transpiration effects in helium and argon are described very well by the empirical expression of Takaishi and Sensui (1963). Considering the small temperature difference involved in the present measurements the uncertainty in the application of this expression is at most 0.4%.

The gas purity of the helium and argon used in these measurements was 99.999%.

The total systematic error in the measured cross section may then be quantified as follows. As mentioned previously, the error due to forward scattering is estimated to be less than 0.1%. We take the effective cell length (gas length) to be equal to the geometrical length, and assume an error of 1% in this approximation, although the work of Mathur *et al* (1975) suggests it should be significantly smaller. The uncertainty

in the temperature measurement using PRT is 0.3%. The stainless-steel ball used in the spinning-rotor viscosity gauge was calibrated by the Deutscher Kalibrierdienst (DKD 2701), who quote a calibration uncertainty of 1.6% for the pressure range covered in this work. An additional uncertainty of up to 0.4% results from other aspects of the SRG operation, such as the determination of the ball offset (McCulloh *et al* 1985). Given the precautions outlined in the previous section, non-linearities in the electron detection and amplification system were estimated to be less than 0.5%. The error due to the uncertainty in the energy scale at high energies (greater than 1.5 eV) is best assessed by considering the effect on the measured cross sections. It will be most pronounced where the energy dependence of the cross section is strongest. Our calculations indicate a worst possible error from this effect of 0.66%, which occurs in the 6–10 eV energy range for argon.

Using these values for the systematic uncertainties we obtain a total systematic error of ±2.2% (1 SD) if the errors are considered to be uncorrelated and are added in quadrature. For a given scan, the statistical error in the derived cross section is obtained by adding in quadrature the random counting errors and the standard deviation of the pressure measurements used in the mean pressure determination. The cross section measurement for a particular experimental run is obtained by taking the weighted mean of the cross sections obtained in the individual scans, and the corresponding error is simply the error in the weighted mean. The overall absolute uncertainty in the final cross sections is obtained by adding the statistical and systematic error.

5. Results and discussion

5.1. Helium

Our measurements of the total electron scattering cross section in helium are presented in table 1 at selected energies between 0.1 and 20 eV. In figures 5(*a*) and 5(*b*) the

Table 1. Measured total cross section in helium. Errors are ±3% (1 SD) at all energies except 0.1 eV, where the error is ±3.75%.

Energy (eV)	σ_T (10^{-16} cm^2)	Energy (eV)	σ_T (10^{-16} cm^2)
0.10	5.52	0.85	6.07
0.12	5.65	0.90	6.07
0.14	5.73	0.95	6.08
0.16	5.73	1.0	6.08
0.18	5.80	1.25	5.99
0.20	5.83	1.50	6.02
0.25	5.87	2.0	5.88
0.30	5.99	3.0	5.70
0.35	5.95	4.0	5.47
0.40	5.98	5.0	5.26
0.45	6.03	6.0	5.06
0.50	6.03	8.0	4.67
0.55	6.03	10.0	4.30
0.60	6.02	12.0	3.96
0.65	6.04	14.0	3.67
0.70	6.03	16.0	3.41
0.75	6.05	18.0	3.17
0.80	6.07	20.0	2.99

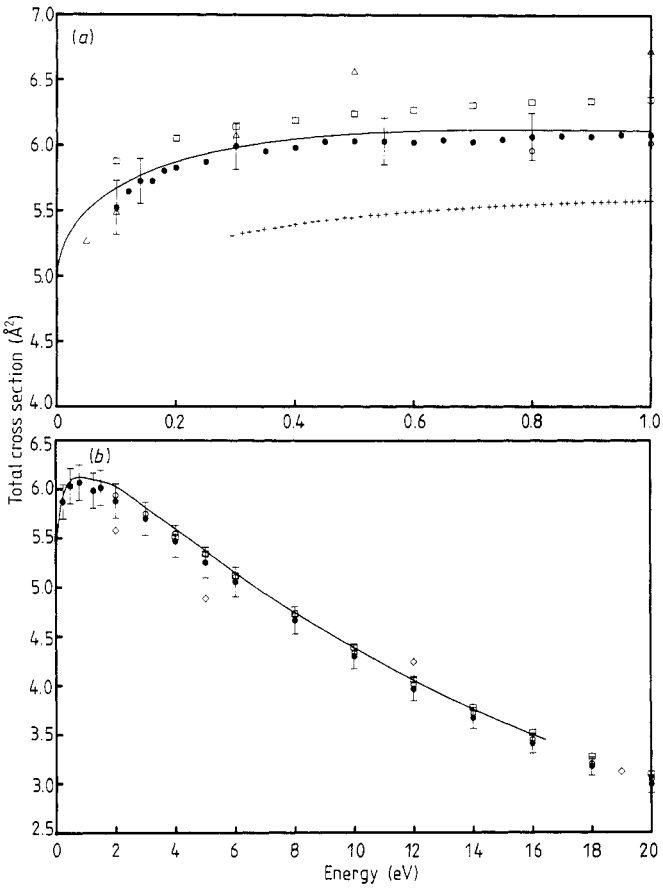

Figure 5. (*a*) Low-energy total cross section in helium (in Å^2). ●, present results; □, Ferch *et al* (1980); ○, Jones and Bonham (1982); △, Gus'kov *et al* (1978); +++, Golden and Bandel (1965); ——, Nesbet (1979). (*b*) Total cross section in helium at 0.1–20 eV (in Å^2). ●, present results; ○, Jones and Bonham (1982); □, Nickel *et al* (1985); ◇, Golden *et al* (1984); ——, Nesbet (1979).

data are compared with other experimental results, as well as with the theoretical calculation of Nesbet (1979). At low energies (figure 5(*a*)) the agreement between the present data and the theoretical calculation of Nesbet is excellent, in general within 2%. A comparison of the present results with the recent experiment of Ferch *et al* (1980) indicates satisfactory agreement, with their results lying approximately 3–5% higher and the quoted error bars on the two data sets overlapping by 1.5%. Above 0.5 eV the agreement between the present data and those of Jones and Bonham (1982) is also good (within 2%). The measurements of Jones and Bonham were prompted by improvements in the experimental method and apparatus used by Kennerly and Bonham (1978), and in general confirm the latter results. At 2 eV and below, the results of Kennerly and Bonham are higher than those obtained by Jones and Bonham, but still lie within the error bars quoted by Jones and Bonham. In the interest of clarity the data of Kennerly and Bonham are not shown in figures 5(*a*) and (*b*). The earlier measurements of Golden and Bandel (1965) lie well below the other experimental and theoretical values in this energy region. The data of Gus'kov *et al* (1978) are in good

agreement with the present measurements at lower energies (within 1.5%) but are higher (about 10%) at energies above 0.5 eV.

At energies above 1 eV (figure 5(*b*)) the present results are in good agreement with the results of Jones and Bonham (1982) and Nickel *et al* (1985), the error bars on our data exhibiting substantial overlap with those of both these data sets. The measurements of Kauppila *et al* (1977) from 1.5-20 eV and Blaauw *et al* (1980) from 16-20 eV are also in good agreement with the present data but are not shown in figure 5(*b*), again in the interest of clarity. The recent results of Golden *et al* (1984), obtained from a phaseshift analysis of relative differential cross sections, are about 5-7% lower than the present results at 2 and 5 eV, and about 7% higher at 12 eV. The error bars of the two data sets overlap at 2 and 5 eV but not at 12 eV and the energy dependence of the total cross section of Golden *et al* (1984) is not consistent with the present measurements or the majority of other recent measurements. The cross section results of Charlton *et al* (1980) (not shown) also exhibit a somewhat different shape from the other results. The present results exhibit good agreement with the theoretical curve of Nesbet, the data lying approximately 1.5-3% below the theoretical results.

In general, the present results are in good agreement with the results of Kauppila *et al* (1977), Kennerly and Bonham (1978), Blaauw *et al* (1980) and Jones and Bonham (1982), and are in reasonable agreement with the results of Nickel *et al* (1985) (which are in excellent agreement with the theoretical values).

5.2. Argon

The present total cross sections in argon, and the associated errors, are presented in table 2 for the energy range 0.12-20 eV. The data are shown graphically in figures

Table 2. Measured total cross section in argon.

Energy (eV)	σ_T (10^{-16} cm^2)	±Error (1 SD) (%)	Energy (eV)	σ_T (10^{-16} cm^2)	±Error (1 SD) (%)
0.12	1.037	6.4	0.65	0.555	3.2
0.13	0.844	5.4	0.70	0.629	3.1
0.14	0.778	4.6	0.80	0.756	3.0
0.15	0.680	5.0	0.90	0.934	3.0
0.16	0.646	4.3	1.00	1.07	3.1
0.17	0.581	4.0	1.50	2.19	3.0
0.18	0.553	4.5	2.00	3.12	3.0
0.19	0.526	4.4	3.00	4.96	3.0
0.20	0.500	4.1	4.00	6.82	3.0
0.25	0.334	4.6	5.00	8.81	3.0
0.30	0.313	3.7	6.00	11.13	3.0
0.34	0.318	3.5	8.00	15.66	3.0
0.36	0.318	3.6	10.0	20.06	3.0
0.40	0.309	4.2	12.0	22.84	3.0
0.45	0.328	3.7	14.0	23.24	3.0
0.50	0.374	3.5	16.0	21.93	3.0
0.55	0.437	3.1	18.0	19.97	3.0
0.60	0.487	3.2	20.0	18.30	3.0

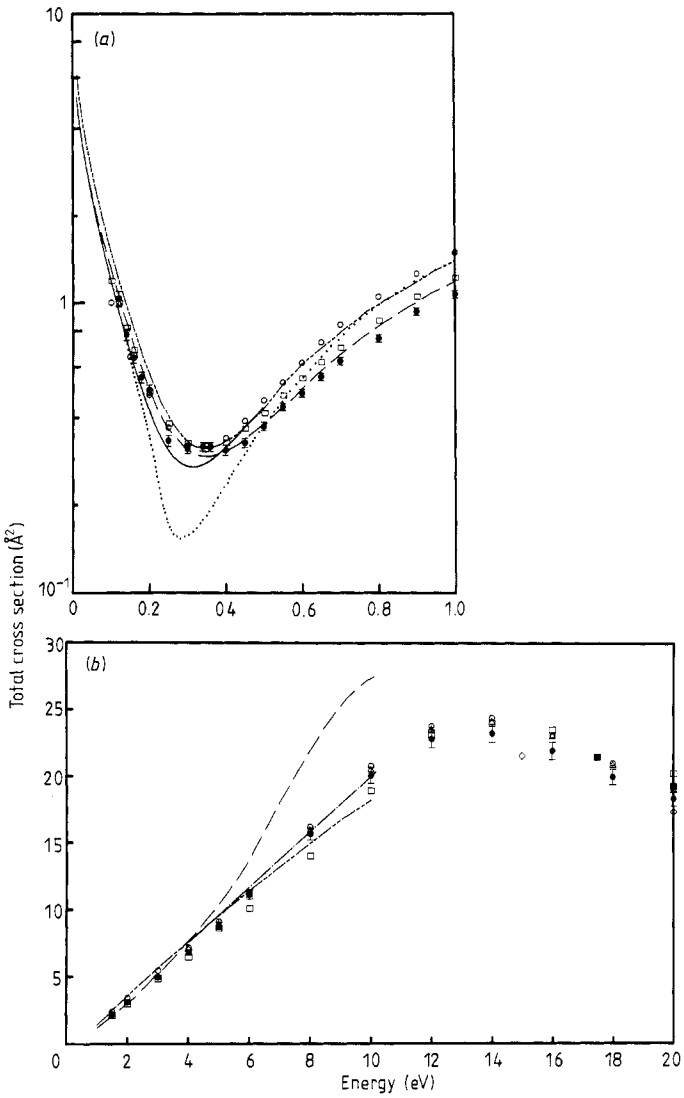

Figure 6. (*a*) Total cross section in argon at 0-1.0 eV (in Å^2). ●, present results; □, Ferch *et al* (1985); ○, Jost *et al* (1983); · · · · ·, Golden and Bandel (1966); ——, swarm analysis of Haddad and O'Malley (1982); - - -, McEachran and Stauffer (1983); — · · —, Bell *et al* (1984). (*b*) Total cross section in argon at 1-20 eV (in Å^2). ●, present results; □, Ferch *et al* (1985); ○, Jost *et al* (1983); △, Nickel *et al* (1985); ◇, Kauppila *et al* (1981); ■, Wagenaar and de Heer (1985); - - -, McEachran and Stauffer (1983); — · —, Fon *et al* (1983); — · · —, Bell *et al* (1984).

6(*a*) (0.1-1.0 eV) and 6(*b*) (1.0-2.0 eV) where comparison is also made with other theoretical and experimental results. At low energies the cross section exhibits a prominent Ramsauer-Townsend (RT) minimum, the existence of which is well known. Both the magnitude and position of the minimum in the cross section, as determined from these measurements, agree to within 3% with two recent experiments (Jost *et al* 1983, Ferch *et al* 1985) and also with the early results of Ramsauer and Kollath (1929)

(not shown in figure 6(*a*)). They are not in agreement with the results of Golden and Bandel (1966) and Gus'kov *et al* (1978) both of which indicate an RT minimum which has a smaller magnitude (about 0.15 $Å^2$) and which occurs at a lower energy (0.280 eV). The dominance of the p-wave contribution to the total cross section in the region of the RT minimum results in a significant enhancement of forward scattering. It is possible that the measurements of Golden and Bandel (1966) and Gus'kov *et al* (1978) are too low in this energy region because of inadequate discrimination against forward-scattered electrons (see also Ferch *et al* 1985). It is also unlikely that the present results (and those of Ferch *et al* and Jost *et al*) are too high because of poorer energy resolution. The energy resolution of the TOF spectrometer at 0.4 eV is estimated to be less than 20 meV whilst the RT minimum is a reasonably broad feature with a 'width' in excess of 150 meV. In general the agreement between the three recent experiments (present, Ferch *et al*, Jost *et al*) at energies below 0.4 eV is within the combined uncertainties. However, between 0.4 and 1 eV the discrepancy between the three data sets increases steadily. At 1 eV the present value is 12% lower than that of Ferch *et al* and 28% lower than that of Jost *et al*. Considering the rather small uncertainties in both the measured cross section and energy in each of the data sets, this disagreement is somewhat mystifying and rather disturbing. Two recent calculations are also compared with the experimental data in figure 6(*a*). The polarised-orbital approach employed by McEachran and Stauffer (1983) results in a cross section which is in rather good agreement (5%) with the present work below 0.7 eV. The cross section obtained from the *R*-matrix calculation of Bell *et al* (1984) is in fair agreement with the present data, being higher by at least 5%, and up to 20%, throughout the energy range 0.12–1.0 eV. Bell *et al* adjusted the energy of one of the bound states used in their code in order to reproduce the scattering length and RT minimum position as found experimentally by Golden and Bandel (1966) and Gus'kov *et al* (1978). As will be shown in the next section, the scattering length determined by these experiments may be too high by as much as 15% and, as indicated above, the RT minimum is too low, both in magnitude and energy.

At higher energies (figure 6(*b*)) comparison is again made with Jost *et al* (1983) and Ferch *et al* (1985) and the agreement is good (generally within 5%) over the energy range shown (1.5–20 eV), particularly with the data of Jost *et al*. Comparison is also made with the transmission experiments of Nickel *et al* (1985) (4–20 eV), Kauppila *et al* (1981) (15 and 20 eV) and Wagenaar and de Heer (1985) (17.5 and 20 eV). In each case there is substantial overlap of the quoted error bars. Also shown in figure 6(*b*) are the calculations of McEachran and Stauffer (1983), Fon *et al* (1983) and Bell *et al* (1984). As these are all total *elastic* cross section calculations, comparison with experiment is only given for energies below the first excitation threshold (11.55 eV). The *R*-matrix calculation of Fon *et al* differs from that of Bell *et al*, principally by the inclusion in the former of a $\overline{4p}$ pseudo-orbital in the ^1P pseudo-state which is used to describe both polarisation and exchange effects. In general the present results are in good agreement with both calculations except at the higher energies (8–10 eV) where they lie closer to the calculation of Fon *et al*. At lower energies (less than 3 eV) the present results show good agreement with McEachran and Stauffer (1983) but this agreement worsens steadily with increasing energy until at 10 eV the theoretical value is about 35% higher than experiment.

Several total *elastic* cross sections derived from differential scattering measurements also exist for this energy range but for reasons of clarity they have not been included in figure 6(*b*). A good summary of these measurements may be found in Bell *et al* (1984).

5.3. Comparison with swarm measurements

In order to compare the total cross section (σ_T) measurements presented here with the precise momentum transfer cross sections (σ_m) available from electron swarm measurements, we have employed modified effective-range theory (MERT) (O'Malley 1963, O'Malley and Crompton 1980, Ferch *et al* 1985). An argon total cross section (0-0.5 eV) derived from the swarm data of Milloy and Crompton (1977, 1982) through the use of MERT (Haddad and O'Malley 1982) is included in figure 6. MERT has also been applied to the present data in the range 0.12-0.5 eV in order to establish accurately the position and magnitude of the RT minimum. The results of the MERT fit to this work and those of Haddad and O'Malley (1982) and Ferch *et al* (1985) are summarised in table 3. The agreement between the present results and the swarm results is excellent for the scattering length, A, but discrepancies remain in both the position and magnitude of the RT minimum.

Table 3. MERT parameters and the resultant position and magnitude of the Ramsauer-Townsend minimum.

Parameter	This work	Ferch *et al* (1985)	Haddad and O'Malley (1982)
A/a_0	−1.492	−1.449	−1.492
A_1/a_0^3	8.555	8.50	9.104
D/a_0^3	63.84	73.1	64.3
F/a_0^4	−62.99	−115.8	−77.3
RT minimum			
Energy (eV)	0.342 ± 0.005	0.345 ± 0.005	0.311
Magnitude (Å^2)	$0.31^{+0.01}_{-0.02}$	0.311	0.27

In the case of helium we found that the application of MERT was not as straightforward as for argon. It appears that it is not possible to unambiguously determine both the S- and the P-wave phaseshifts, presumably due to the lack of a strong energy dependence in the cross section. We found that, by fixing the P-wave phaseshift (using the calculated values of Nesbet (1979)) and only fitting the S-wave phaseshift, it was possible to obtain a total cross section from the swarm measurements over the energy range 0-0.5 eV. The resultant cross section was in excellent agreement (±1%) with the present results. A similar MERT analysis applied to the present data in the energy range 0.1-0.5 eV yielded a value of 1.16 Å^2 for the e^--He scattering length, in reasonable agreement with the value of 1.19 Å^2 (±2%) obtained by Crompton *et al* (1970) and the value of 1.183 Å^2 obtained by Nesbet (1979).

A comparison of the present results with those of Crompton *et al* (1970) for helium over a wider energy range (up to 12 eV) can be achieved via the theoretical values of Nesbet (1979). We have obtained total cross sections from the swarm σ_m measurements by multiplying the latter by the ratio of (σ_T/σ_m) predicted by the theory. These differ from the present results by 0.1, 2 and 0.9% at 1, 5 and 12 eV respectively.

Acknowledgments

Many people made major contributions to the design and construction of the apparatus used in this work. It is a pleasure to acknowledge the technical skills of Kevin Roberts,

Tom Halstead and John Gascoigne. We are also indebted to the staff of the Electronics Unit, in particular Tony Cullen, Sam Hijazi, Dennis Gibson and Neville Esau for the design and construction of the electron lens power supplies and beam-gating system. The assistance of Tom Rhymes and Peter Smith with the on-line computer control system is gratefully acknowledged. We also thank Dr R W Crompton and Dr M T Elford for their critical reading of the manuscript, and Professor K Jost for providing tabulated cross section values prior to final publication.

References

Baldwin G C and Gaerttner M A 1973 *J. Vac. Sci. Technol.* **10** 215-7
Bell K L, Scott N S and Lennon M A 1984 *J. Phys. B: At. Mol. Phys.* **17** 4757-65
Bertram S 1942 *J. Appl. Phys.* **13** 496-502
Blaauw H J, Wagenaar R W, Barends D H and de Heer F J 1980 *J. Phys. B: At. Mol. Phys.* **13** 359-76
Brode R B 1925 *Phys. Rev.* **25** 636-44
Brüche E 1927 *Ann. Phys., Lpz.* **84** 279-91
Brunt J N H, Read F H and King G C 1977 *J. Phys. E: Sci. Instrum.* **10** 134-9
Charlton M, Griffith T C, Heyland G R and Twomey T R 1980 *J. Phys. B: At. Mol. Phys.* **13** L239-44
Chutjian A and Cartwright D C 1981 *Phys. Rev.* A **23** 2178-93
Crompton R W, Elford M T and Robertson A G 1970 *Aust. J. Phys.* **23** 667-81
Ferch J, Granitza B, Masche C and Raith W 1985 *J. Phys. B: At. Mol. Phys.* **18** 967-83
Ferch J, Raith W and Schröder K 1980 *J. Phys. B: At. Mol. Phys.* **13** 1481-90
Fon W C, Berrington K A, Burke P G and Hibbert A 1983 *J. Phys. B: At. Mol. Phys.* **16** 307-21
Golden D E and Bandel H W 1965 *Phys. Rev.* A **138** 14-21
—— 1966 *Phys. Rev.* **149** 58-9
Golden D E, Furst J and Mahgerefteh M 1984 *Phys. Rev.* A **30** 1247-54
Gus'kov Yu K, Savvov R V and Slobodyanyuk V A 1978 *Sov. Phys.-Tech. Phys.* **23** 167-71
Haddad G N and O'Malley T F 1982 *Aust. J. Phys.* **35** 35-9
Harting E and Read F H 1976 *Electrostatic Lenses* (Amsterdam: Elsevier)
Howard W M 1961 *Phys. Fluids* **4** 521-4
Jones R K and Bonham R A 1982 *Aust. J. Phys.* **35** 559-70
Jost K, Bisling P G F, Eschen F, Felsmann M and Walther L 1983 *Proc. 13th Int. Conf. on the Physics of Electronic and Atomic Collisions (Berlin) 1983* ed J Eichler *et al* (Amsterdam: North-Holland) Abstracts p 91
Kauppila W E, Stein T S, Jesion G, Dababneh M S and Pol V 1977 *Rev. Sci. Instrum.* **48** 822-8
Kauppila W E, Stein T S, Smart J H, Dababneh M S, Ho Y K, Downing J P and Pol V 1981 *Phys. Rev.* A **24** 725-42
Kennerly R E 1978 *Rev. Sci. Instrum.* **48** 1682-8
Kennerly R E and Bonham R A 1978 *Phys. Rev.* A **17** 1844-54
Kisker E 1982 *Rev. Sci. Instrum.* **53** 114-6
Land J E and Raith W 1974 *Phys. Rev.* A **9** 1592-1602
Mathur B P, Field J E and Colgate S O 1975 *Phys. Rev.* A **11** 830-3
McCulloh K E, Wood S D and Tilford C R 1985 *J. Vac. Sci. Tech.* A **3** 1738-41
McEachran R P and Stauffer A D 1983 *J. Phys. B: At. Mol. Phys.* **16** 4023-38
Milloy H B and Crompton R W 1977 *Aust. J. Phys.* **30** 51-60
—— 1982 *Aust. J. Phys.* **35** 105-6
Nesbet R K 1979 *Phys. Rev.* A **20** 58-70
Nickel J C, Imre K, Register D F and Trajmar S 1985 *J. Phys. B: At. Mol. Phys.* **18** 125-33
O'Malley T F 1963 *Phys. Rev.* **130** 1020-9
O'Malley T F and Crompton R W 1980 *J. Phys. B: At. Mol. Phys.* **13** 3451-64
Poulter K F, Rodgers M J, Nash P J, Thompson T J and Perkin M P 1983 *Vacuum* **33** 311-6
Raith W 1976 *Adv. At. Mol. Phys.* **12** 281-373
Ramsauer C and Kollath R 1929 *Ann. Phys., Lpz* **3** 536-64
Read F H 1969 *J. Phys. E: Sci. Instrum.* **2** 679-84
—— 1970 *J. Phys. E: Sci. Instrum.* **3** 127-31

Register D F, Trajmar S and Srivastava S K 1980 *Phys. Rev.* A **21** 1134–51
Takaishi T and Sensui Y 1963 *Trans. Faraday Soc.* **59** 2503–14
Wagenaar R W and de Heer F J 1985 *J. Phys. B: At. Mol. Phys.* **18** 2021–36
Weyhreter M 1983 *Diplomarbeit* Universität Kaiserslautern (unpublished)